ISSN 1995-0780, Nanotechnologies in Russia, 2017, Vol. 12, Nos. 1–2, pp. 86–97. © Pleiades Publishing, Ltd., 2017.
Original Russian Text © M.Yu. Tsvetkov, V.I. Yusupov, P.S. Timashev, K.M. Golant, N.V. Minaev, V.N. Bagratashvili, 2017, published in Rossiiskie Nanotekhnologii, 2017, Vol. 12, Nos. 1–2.

Improving the Efficiency of Laser-Induced Backside Wet Etching of Optically Transparent Materials as a Result of Generation of Carbon and Silver Nanoparticles

M. Yu. Tsvetkov[a], V. I. Yusupov[a], P. S. Timashev[a], K. M. Golant[b], N. V. Minaev[a], and V. N. Bagratashvili[a,c]

[a] *Federal Research Center "Crystallography and Photonics," Russian Academy of Sciences, Moscow, 119333 Russia*
[b] *Kotel'nikov Institute of Radioengineering and Electronics, Russian Academy of Sciences, Moscow, 125009 Russia*
[c] *Chemistry Department, Moscow State University, Moscow, 119991 Russia*
**e-mail: iouss@yandex.ru*

Received June 3, 2016; in final form, October 13, 2016

Abstract—The processes of laser-induced backside wet etching (LIBWE) and microstructuring of silicate glass by laser impulses with a wavelength of 527 nm and a duration of about 5 ns have been studied in different aqueous solutions that provide different etching modes, namely, volume (in a solution of dye), volume + surface (in a solution of dye and polyethylene glycol (PEG)), and surface modes (in an aqueous solution of $AgNO_3$). It is shown that the etching rate and the quality of the obtained structures depend on two different processes: the chemical etching of the material surface by water in the supercritical state (fluid produced at fast laser heating) and the shockwave or cavitational destruction of a material. The LIBWE rate and the quality of the formed microstructures are determined by a dominating mechanism of the process. In the case of an aqueous dye solution, the shockwave and cavitational destruction dominates, which makes it impossible to create well-replicated craters and tracks with smooth walls. Upon the addition of PEG to a solution of dye and, especially, upon using an aqueous solution of the silver precursor ($AgNO_3$), the laser-induced processing of carbon or silver nanoparticles gives rise to a strong absorption on the surface of the formed structure, the undesirable cavitational destruction of a material is suppressed, and the process of etching of the glass surface by supercritical water becomes a dominating mechanism of LIBWE. As a result, it is possible to create highly effective and well-reproducible LIBWE technology for the fabrication of precision optical microstructures on the surface of advanced optical materials on the basis of high-performance and reliable lasers with a wavelength of 527 nm.

DOI: 10.1134/S1995078017010141

INTRODUCTION

Laser micro- and nanotechnologies are widely used for the generation of structures on the surface of different materials (see, for example, [1–5]). One advanced and rapidly developing approach to the fabrication of microstructures on the surface of optically transparent materials is liquid etching induced by a laser beam on the backside surface of transparent materials (laser-induced backside wet etching, LIBWE) [6] (proposed in [7, 8]). For the implementation of such a process, pulsed laser radiation is focused on the backside surface of a transparent sample, which is in contact with a strongly- absorbing liquid, causing the local removal of a near-surface layer of the material. The LIBWE process is characterized by relatively low threshold densities of the radiation energy (about 0.5 J/cm^2 for molten quartz) and by a low roughness of the etched surface (less than 10 nm rms) [9]. The LIBWE rate is determined by the nature of a material, the composition of the liquid, and the parameters of pulsed laser radiation.

Eximer UV lasers and organic liquids or solutions that strongly absorb UV radiation were used in the first LIBWE experiments [7, 8]. In the subsequent studies, LIBWE was implemented by using other types of lasers as well, namely, solid-state lasers with diode pumping [10, 11], lasers on copper vapors [12, 13], lasers with super-short impulses [14, 15], etc. The possibility of processing optical materials that are not transparent for UV light, such as silicate glass and optical ceramics, is a major advantage of the application of visible-band lasers for LIBWE.

Organic dyes or organic solvents such as benzene, toluene, and tetrachloromethane are traditionally used as absorbing media [7, 8, 16]; however, there are publications on the use of inorganic solutions [17–19]. It was also suggested to use molten metals to increase

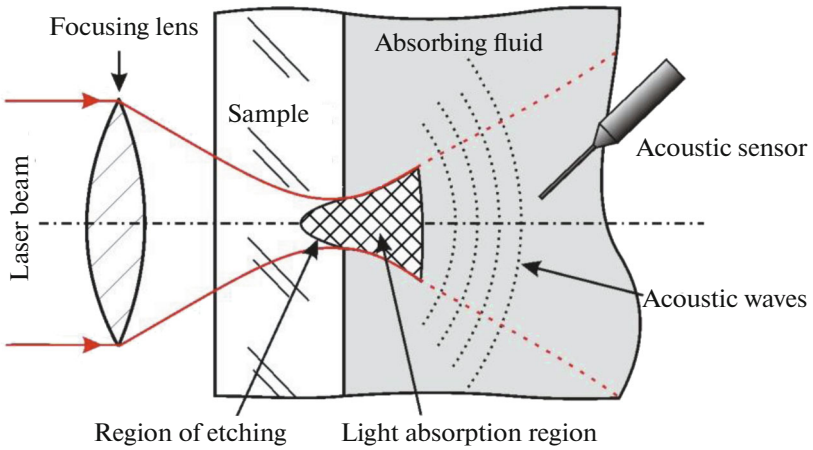

Fig. 1. (Color online) Scheme of laser liquid etching of the surface of an optically transparent sample by focused laser radiation.

the efficiency of etching [20–22]. The method of laser-induced plasma ablation (laser-induced plasma-assisted UV ablation LIPPA) was developed [23, 24]. Methods of laser-induced dry etching from the backside (laser-induced backside dry etching LIBDE) [25, 26] and laser etching in the presence of an absorbing surface layer (laser etching at surface adsorbed layer LESAL) were also proposed [27]. In these methods, a thin layer of metal and absorbing toluene vapors, respectively, were used as a medium for absorbing the laser radiation. The use of microstructured media, in particular, SiO_2 microspheres coated with a thin layer of gold for laser etching, is of considerable interest [28].

Mechanisms of the LIBWE process and the problems related to an increase in its efficiency were studied in a whole series of works (see, for example, [29–33]). A number of physical and chemical processes (nonlinear absorption of radiation, thermal and hydrodynamic processes, photo- and thermochemical reactions, the formation of a supercritical fluid, the formation and collapse of bubbles, melting, evaporation, etc.) take place in the laser-focusing spot on the solid–liquid boundary, giving rise to the removal (etching) of the sample material.

The aim of this study is to develop an LIBWE method allowing one to provide a highly effective and well-reproducible process for the generation of microstructures in optical materials by using accessible and effective pulse lasers in the green region of the visible light.

EXPERIMENTAL

Experimental Equipment and LIBWE Techniques

Our experimental equipment for the laser liquid etching of optically transparent materials is described in detail in [32, 33]. The principal scheme of the experiment is shown in Fig 1. The second harmonics of a TECH-527 Basic diode-pumped solid-state laser (Laser-compact, Russia) with a wavelength of $\lambda = 527$ nm, laser pulse duration of about 5 ns, maximum energy per pulse of 250 μJ, and beam deviation angle of less than 3 mrad was used for the irradiation of samples. The optical scheme of the device makes it possible to form a Gaussian-profile laser beam with specified energy and geometric parameters (see below). Next, the radiation is directed to a lens via a spectrally selective (dichroic) mirror and focused to a point on the boundary between a fluid and the backside surface of a transparent sample. The use of such a mirror allows one to register the image of the surface spot in the etching zone by an EXCCD USB 2.0 camera (ToupTek) upon illumination with white light from a lamp. The visualization of the image on a computer monitor affords the accurate alignment of the sample and makes it possible to monitor the surface etching process online. The control over the laser beam, as well as the control and diagnostics of the etching process, is implemented with a computer.

Silicate glass slides were used as samples for the LIBWE process. The glass plate to be treated was installed as a front wall of the disassemblable cuvette filled with a strongly absorbing fluid (see [32]). The cuvette with the sample was placed on an 8MT167-100 three-axis XYZ translation stage (Standa) with a positioning accuracy of no worse than 0.5 μm. An LMH-10X-532 (Thorlabs) 10 × lens with NA = 0.25 was used for focusing the radiation to the rear surface of the plate.

Saturated aqueous solutions of Amaranth food dye (Sigma-Aldrich) [34, 35] and silver nitrate ($AgNO_3$) were used as strongly absorbing fluids in the LIBWE experiments. The experiments were performed at different solution concentrations. The foremost results were obtained for solutions with concentrations close to the maximum solubility of substances, specifically, for a 0.1 mol/dm^3 solution of Amaranth and for a

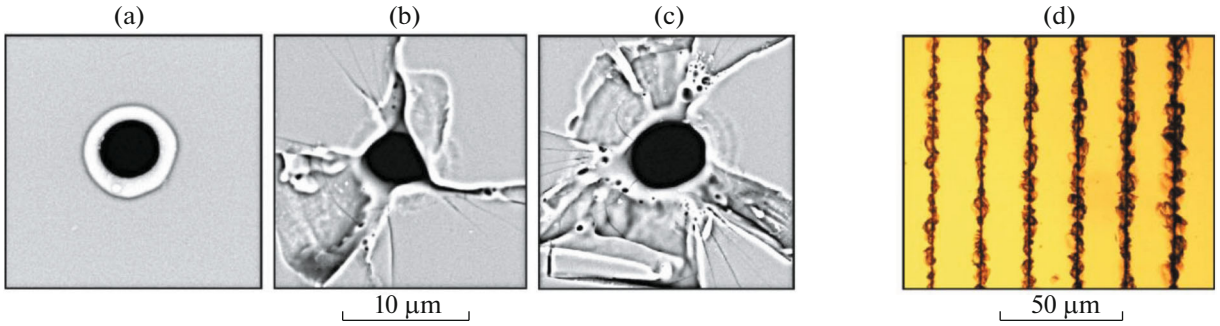

Fig. 2. (Color online) SEM images of (a–c) craters and optical images of (d) tracks produced on the surface of a transparent sample during the LIBWE process with using a saturated dye solution as an absorbing medium for different values of the laser radiation energy density, Φ; the Φ value is increased from left to right, as follows: 100, 200, and 400 J/cm^2 for craters (single-pulse mode) and from 50 to 100 J/cm^2 for tracks.

5 mol/dm^3 solution of $AgNO_3$. To study the influence of surfactants on the etching process, polyethylene glycol (PEG500) in concentrations of up to 50 vol % was added to the solutions.

The absorption spectra of dye solutions, as well as the optical extinction spectra of a suspension of plasmonic particles produced in an aqueous solution of $AgNO_3$ as a result of LIBWE, were measured using a Cary-50 spectrophotometer (Varian). The absorption coefficient of dye at a wavelength of 527 nm was 2×10^3 cm^{-1} in the case of using the saturated solution. This ensured a laser radiation absorption rate of about 90% in the fluid layer with a thickness of about 10 μm.

The in situ diagnostic of the LIBWE process was performed with the use of optoacoustic methods [32, 33, 36]. Acoustic signals were recorded using a needle hydrophone (Precision Acoustics) with a broadband (100 MHz) preamplifier. The hydrophone had flat (±4dB) spectral characteristics in the range from 200 kHz to 15 MHz and a sensitivity of 850 nV/Pa. The sensitive face of the needle hydrophone was placed into a liquid at a distance of 7 mm from the laser exposure. The signals from the hydrophone were recorded on a GDS 72304 memory oscillograph (GW Instek) with a bandwidth of 300 MHz. The pressure value was recalculated assuming the spherical divergence of the acoustic wave to a distance of 10 μm from the laser focus location.

The geometry, shape, and characteristics of the surface of craters produced in the samples were studied using optical, scanning electron (SEM), and atomic force (AFM) microscopies. The optical images of craters produced in the transparent specimen as a result of LIBWE at different laser pulse energy densities (Φ) were obtained using an HRM-300 optical microscope (Huvitz, Korea) with a feature of the visualization of three-dimensional surface topography. The SEM images of craters were obtained on a Phenom ProX scanning electron microscope equipped with an integrated system of energy-dispersive elemental analysis. An INTEGRA Terma scanning probe nanolaboratory (NT-MDT, Russia) and measurement techniques described in [32] were applied for producing the AFM images. Raman spectral studies were performed on a Nicolet Almega Raman-scattering spectrometer.

RESULTS AND DISCUSSION

The experiments on the laser structuring of silicate glass samples were carried using laser radiation in the energy range from 0.5 to 50 μJ at a pulse sequence frequency of 1 kHz. The focus parameters of a Gaussian laser beam are determined by the diameter of the beam ahead of a focusing lens and by the parameters of focusing optics [37]. The diameter of the beam in our case was 4 mm, which allowed us to form a spot with the following parameters in the focus area on the boundary between the sample and the absorbing fluid: a minimum laser beam waist diameter of 3.4 μm (with regard to the 1/*e* level) and a waist depth of 33.5 μm. The laser pulse energy density, Φ, on the surface of the sample was in the range of from 5.5 to 550 J/cm^2.

LIBWE in a Saturated Solution of Dye

The SEM and optical microimages of typical craters and tracks on the silicate glass surface, which were obtained in the process of LIBWE upon using a saturated aqueous solution of Amaranth dye as an absorbing liquid, are shown in Fig. 2. Such a mode of LIBWE irradiation was used in this case, when approximately 90% laser radiation is absorbed by a liquid layer near the sample surface with a thickness of 10 μm. Let us note that this exceeds the laser beam diameter at the surface (3.4 μm) by nearly three times. Therefore, we call this mode the volume-absorption mode.

As is shown by our experiments, the interaction of laser radiation with a saturated solution of dye can be "soft" (at $\Phi < 50$ J/cm^2) or "hard" ($\Phi > 100$ J/cm^2)

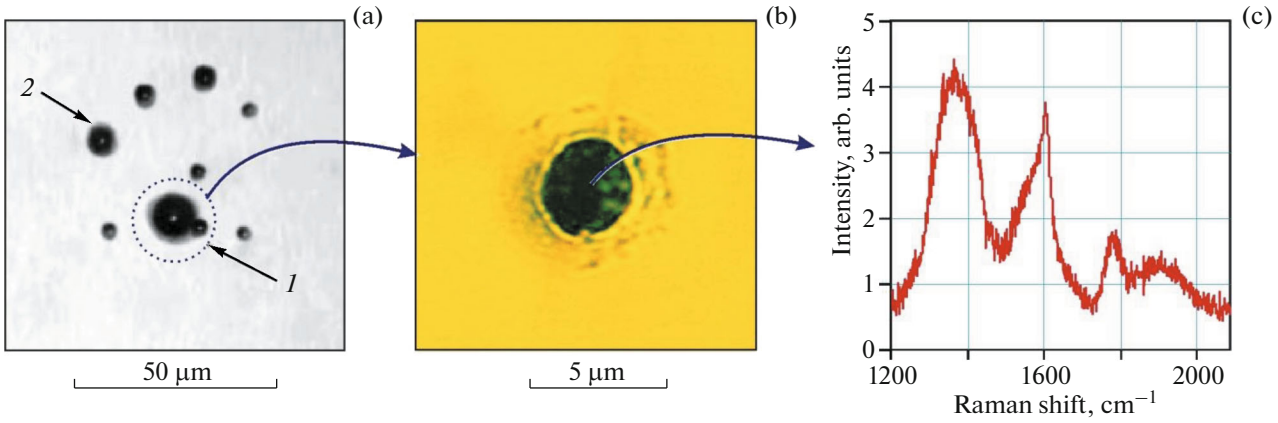

Fig. 3. (Color online) Laser-induced production of carbon in the process of laser etching of a crater on the surface of an optically transparent sample when PEG is added into an aqueous dye solution, as illustrated (a) by the image obtained in the process of crater etching, in which (*1*) the focusing spot of laser radiation is marked by a circle and (*2*) the bubbles coated with carbon nanoparticles produced in the LIBWE process are seen; (b) by the optical image of the crater produced in the result of this process, which is covered with generated carbon nanoparticles (the rings around the crater also consist of nanocarbon); and (c) by the Raman scattering spectrum confirming the presence of carbon nanoparticles on the crater surface.

[32], depending on the character of the laser imprint (crater) on a transparent sample and on the character of the optoacoustic response. Upon soft exposure (Fig. 2a), a regularly shaped crater with a diameter of 3 to 4 μm at the sample surface level is formed on the surface of silicate glass. We associate such a mode of material removal with etching by supercritical water generated near the surface of glass upon rapid laser heating of an absorbing fluid [33]. When the laser radiation energy density, Φ, is increased, the exposure becomes hard. In this case, craters with uneven edges and extensive cracks radiating from them are formed (Figs. 2b, 2c). The formation of irregularities and cracks is associated with the shockwave destruction of material, which is caused by the cavitation accompanied by high amplitudes of the pulse pressure (about 10^9 Pa at $\Phi \sim 100$ J/cm^2) registered by optoacoustic methods [32, 33]. Significant fluctuations of the pulse pressure amplitude cause the poor reproducibility of emerging craters under the equal conditions and low quality of the formed tracks (Fig. 2d). An attempt to get higher quality structures by suppressing the cavitation as a consequence of reducing the Φ value gives rise to a drastic decrease in the etching rate. The track quality remains low in this case, which is explained by the fluctuational nature of cavitation continuing to play an important role in the LIBWE mechanism under the volume radiation absorption mode.

In the multipulse mode, the borderline of the transition from the soft to hard mode shifts toward lower energy densities. This is connected with the fact that the second and subsequent laser pulses upon etching affect the modified surface of an already formed crater, which itself promotes the additional absorption of laser radiation. The above circumstance significantly limits the etching rate upon using the aqueous solutions of dyes as absorbing fluids. Most importantly, we have never succeeded in the formation of tracks with smooth walls by varying the laser exposure energy (Fig. 2d).

LIBWE in the Presence of Polyethylene Glycol

We managed to somewhat suppress the undesirable cavitational destruction of the sample material by carrying out the LIBWE process in an aqueous dye solution with added PEG500 polyethylene glycol (PEG). The idea of adding PEG to an aqueous dye solution appeared due to the desire to reduce the liquid surface tension and, thereby, suppress the unwanted cavitational destruction of the material. It was established from the experiments that the addition of PEG, in addition to a decrease in the cavitation, gives rise to an increase in the rate of formation of structures on the silicate glass surface. As is seen from Fig. 3, carbon nanoparticles are intensively generated in this case as a result of the laser etching process (due to the pyrolysis of PEG), covering the surface with numerous microbubbles (Fig. 3a) and forming craters (Fig. 3b).

The generation of nanosized carbon in a cuvette with the irradiated sample is directly confirmed by independent Raman spectroscopy measurements. As is seen from Fig. 3c, the local maximums in the ranges from 1300 to 1430 and from 1540 to 1620 cm^{-1} are distinguished in the Raman spectrum of the laser crater, which correspond to different forms of nanosized carbon [38, 39]. These Raman bands were not registered before the laser exposure.

Let us note that rather weak nanocarbon bands were also observed after the LIBWE processing in an aqueous dye solution (without the addition of PEG), which we associate with the thermal destruction of dye

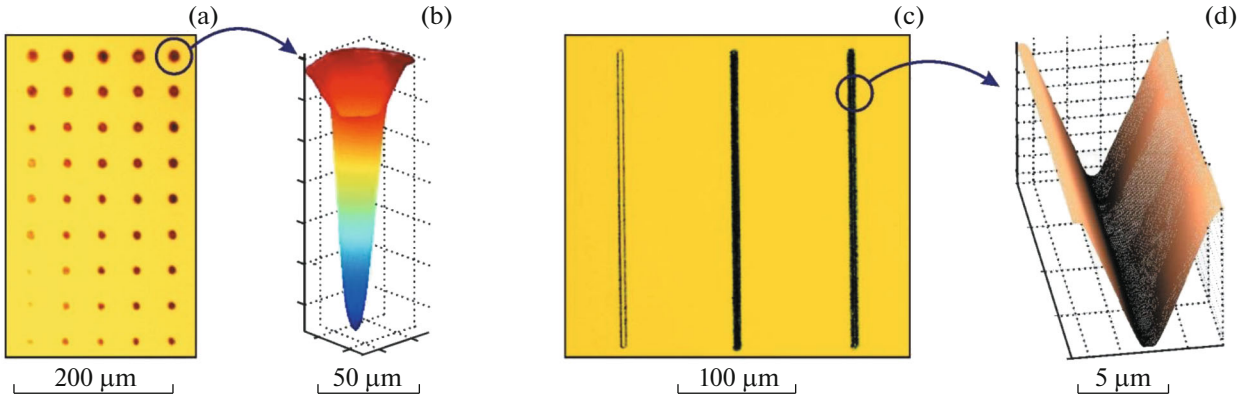

Fig. 4. (Color online) Optical images of the array of (a) laser craters and (c) laser tracks produced in silicate glass during the LIBWE process in an aqueous $AgNO_3$ solution at different laser exposure parameters, and examples of the 3D images of a (b) crater and (d) track; the laser exposure parameters are as follows: (a) for the crater arrays, the Φ value is increased in the vertical direction from 45 to 100 J/cm^2, and the number of pulses is increased from left to right from 250 to 4000 impulses; (c) for the tracks, 20 scans at Φ = 4.5 J/cm^2, 40 scans at Φ = 4.5 J/cm^2, and 20 scans at Φ = 10 J/cm^2 in sequence from left to right.

(the concentration of which, according to our estimation, is higher by one to two orders of magnitudes in comparison with the LIBWE process in the presence of PEG).

The quality of the laser craters and tracks produced by LIBWE in an aqueous dye solution with the addition of PEG is already significantly higher than in the case of LIBWE in an aqueous solution of pure dye. At the same time, the LIBWE rates achieved under the soft mode (in the absence of the shockwave destruction of structures) are still significantly lower than the rates obtained upon using the UV laser radiation for LIBWE [40] (let us recall that we use the laser radiation with λ = 527 nm for LIBWE). An attempt to significantly increase the etching rate by increasing the laser pulse energy density always gave rise to the deterioration of the quality of laser tracks due to the shockwave (cavitational) destruction.

LIBWE in an Aqueous Solution of $AgNO_3$

A significant increase in the LIBWE rate with avoiding the unwanted shockwave destruction of resulting structures was achieved by using an aqueous solution of $AgNO_3$ as a working fluid. The laser craters (Figs. 4a, 4b) and tracks (Figs. 4c, 4d) obtained in this mode have very good quality (unlike those given in Fig. 2) and directly indicate the absence of unwanted shockwave fractures. The achieved etching rates (up to 10 nm/pulse) and high-quality craters and tracks generated by a laser with λ = 527 nm are comparable to those obtained by the LIBWE processing in hydrocarbon solutions with the use of UV lasers [40].

According to our studies, nanoparticles and agglomerates of metallic silver are intensively generated in this case upon the laser irradiation of an aqueous solution of $AgNO_3$ (see Fig. 5) [41–43]. They are registered as silver islands on the glass surface at the initial stages of laser irradiation (when the laser crater is not yet revealed) (Fig. 5a).

Upon longer laser exposure, metallic silver on the surface of produced craters is well resolved on the SEM images (Fig. 5c) and also registered by energy dispersion spectroscopy (Fig. 5d). Moreover, the formation of silver nanoparticles and agglomerates in the working $AgNO_3$ solution upon completion of the LIBWE process is clearly confirmed by the optical extinction spectrum (Fig. 5b) with a characteristic plasmonic band in the 350- to 500-nm region corresponding to different geometrical shapes and sizes of nanosized silver [44, 45].

Acoustic Measurements during the LIBWE Process

The fragments of characteristic acoustic signals recorded during the LIBWE treatment of silicate glass in different working fluids are shown in Fig. 6. One can see that the maximum pulse pressure amplitudes for the same laser energy density values are registered upon using an aqueous dye solution as a working fluid and the minimal amplitudes upon using a silver precursor solution. In the sequence dye → dye + PEG → $AgNO_3$, the maximum pulse pressure amplitudes are successively decreased as 100% → 30 ± 5% → 10 ± 4% and the root mean square values of the pulse pressure amplitude as 100% → 6 ± 2% → 3 ± 1%, respectively. Therefore, the addition of PEG to an aqueous dye solution and, moreover, the use of an aqueous solution of $AgNO_3$ as a working fluid give rise to a significant decrease in the amplitude of the registered acoustic pulses, directly evidencing a significant suppression in the cavitation.

Let us analyze in more detail the possible mechanisms of LIBWE of glass upon using the following

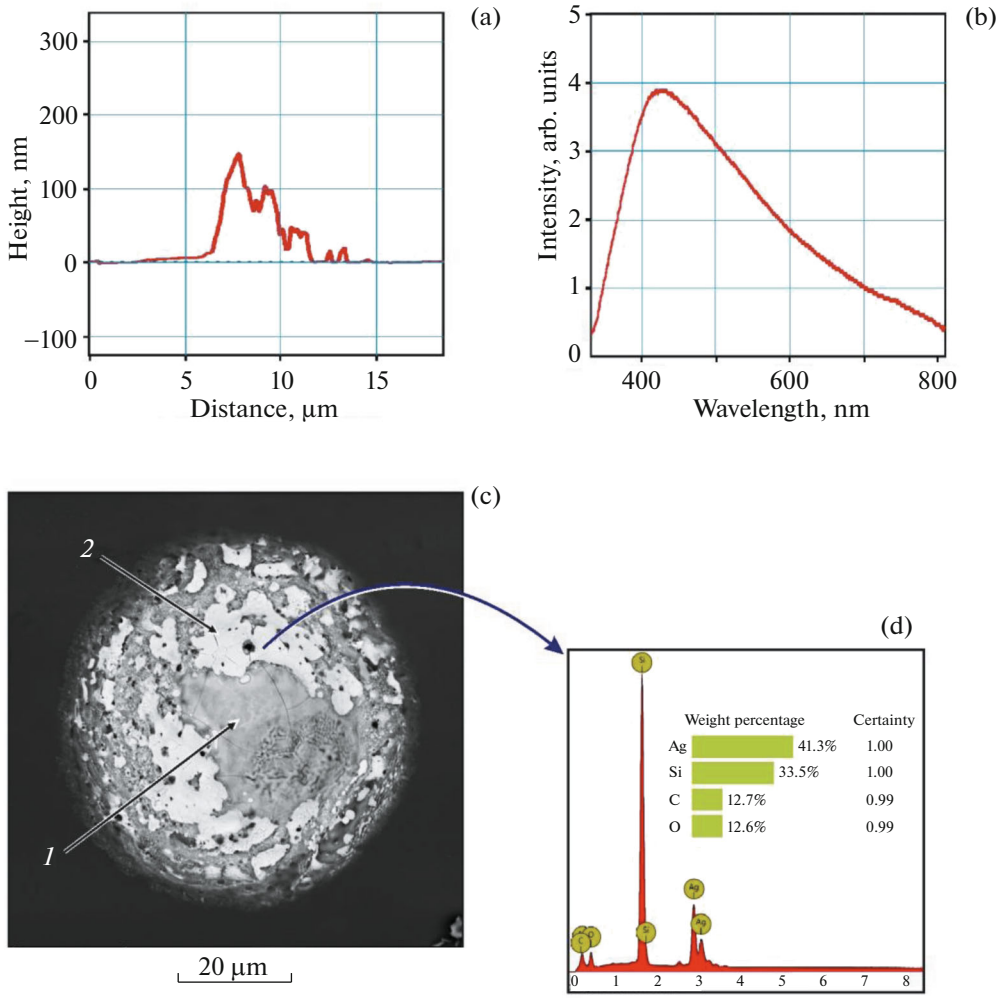

Fig. 5. (Color online) Laser-induced formation of metallic silver during the LIBWE process in an aqueous solution of $AgNO_3$, as illustrated (a) by the AFM profile of the glass surface with a silver layer produced in the area of the laser exposure ($t = 10$ s) at $\Phi = 26$ J/cm^2, (b) by the optical extinction spectrum of a working fluid after the performed LIBWE process with a plasmonic absorption peak related to the presence of produced silver nanoparticles and agglomerates, (c) by the SEM image of a crater in silicate glass with the areas corresponding to (*1*) the crater bottom and (*2*) metallic silver produced on the crater surface, and (d) by the results of energy dispersion elemental analysis.

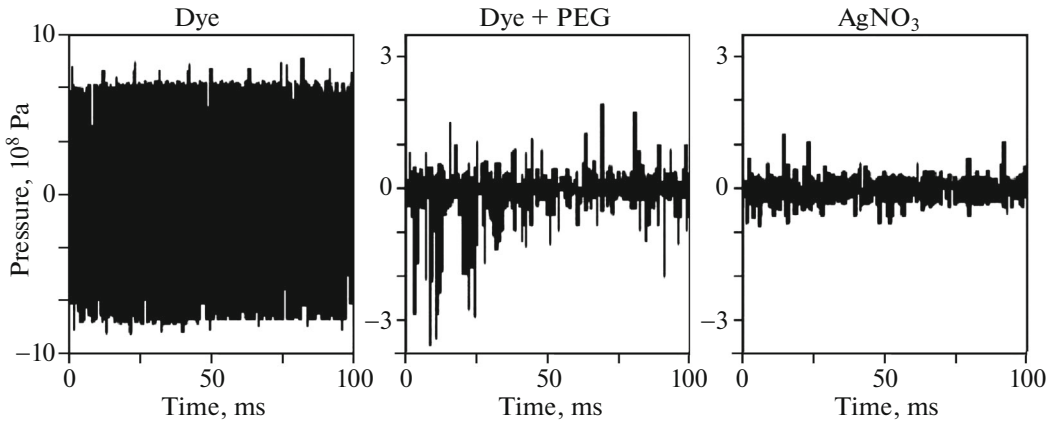

Fig. 6. Fragments of acoustic signals obtained during the LIBWE process in three different working fluids ($\Phi = 100$ J/cm^2).

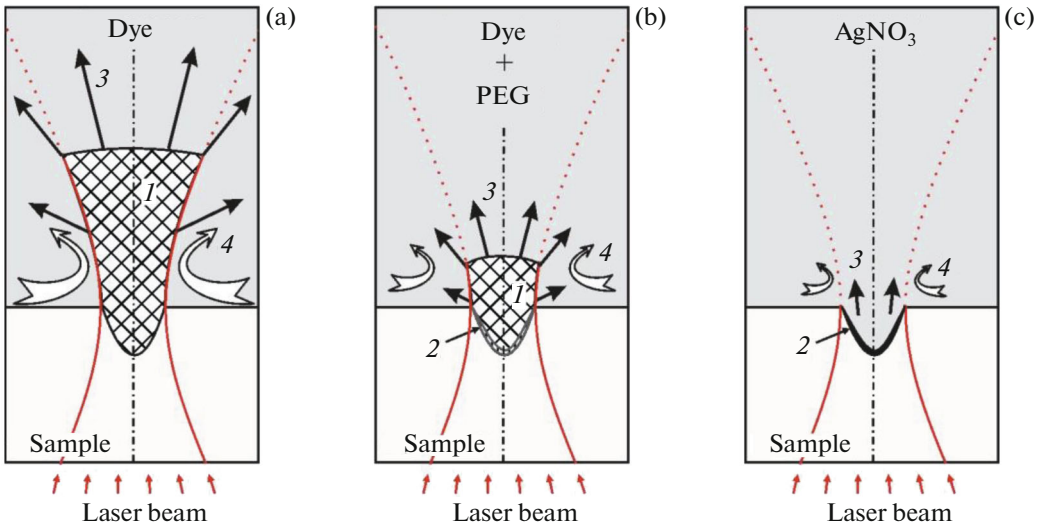

Fig. 7. (Color online) Schematic diagram explaining the action mechanism of the LIBWE process in different working liquid media and containing (*1*) the region of volume absorption of the laser energy, (*2*) the region of surface absorption of the laser energy, (*3*) the directions of the expansion of the area with high temperature and pressure, and (*4*) laser-induced flows in a fluid where the two hyperbolas (red curves) denote the exposure region of pulsed laser radiation focused on the transparent sample/liquid boundary.

three types of fluids: (a) an aqueous solution of dye, (b) an aqueous solution dye and PEG, and (c) an aqueous solution of $AgNO_3$. We believe that the above described differences in the LIBWE rate and in the surface quality of laser craters and tracks produced in silicate glass are explained by different ratios between the volume and surface absorption of laser radiation under these three LIBWE modes. The key processes taking place upon the exposure of a laser pulse focused on the backside surface of an optically transparent sample contiguous with different absorbing fluids are schematically illustrated in Fig. 7.

LIBWE under the Mode of Volume Radiation Absorption

When an aqueous dye solution is used as an absorbing fluid (Fig. 7a), a certain volume of liquid (labeled as 1 in Fig. 7a) is heated up as a result of the absorption of a laser pulse. The volume of this region is determined by the geometric parameters of laser focusing (of the hyperbola in Fig. 7a) and by the distance at which 90% of the laser energy are absorbed, equal to about $2 \times \alpha^{-1} = 10$ μm, where $\alpha = 2 \times 10^3$ cm^{-1} is the absorption coefficient. In our case, almost all the laser energy is absorbed in a volume of about 150 μm^3. At $t = \tau$, where τ is the laser pulse length, the absorption of the energy of a short laser pulse in this volume of liquid eventually gives rise to the consequence that the fluid is heated up to the temperature [7],

$$T = T_0 + \frac{\Phi(1 - \exp(-\alpha d_T^L))}{\rho^G C_p^G d_T^G + \rho^L C_p^L d_T^L}, \quad (1)$$

where T_0 is the initial temperature equal to 300 K; ρ^L is the density; C_p is the specific heat capacity; $d_T = \sqrt{4D_T\tau}$ is the thermal heat-up depth; D_T is the coefficient of thermal conductivity; τ is the laser pulse length; and the L and G upper indices are related to glass and liquid, respectively. Substituting the tabulated values, $\rho^L = 1000$ kg/m^3, $\rho^G = 2500$ kg/m^3, $C_P^L = 4200$ J/(kg K), $C_P^G = 700$ J/(kg K), $D_T^L = 1.4 \times 10^{-7}$ m^2/s, $D_T^G = 3.4 \times 10^{-7}$ m^2/s, and $\tau = 5 \times 10^{-9}$ s into the formula, one can obtain $T \approx 1.7 \times 10^4$ K for $\Phi = 40$ J/cm^2. Thus, the absorption of a laser pulse heats up the fluid volume (labeled as 1 in Fig. 7a) to the temperature, $T \gg T_c$, where T_c is the water critical temperature close to 6.47×10^2 K.

As is known, the explosive boiling of liquid with the formation of a rapidly expanding bubble in the laser exposure area, which cavitationally collapses upon reaching its maximum radius, R_{max}, occurs already at a temperature of $(0.9–1)T_c \approx (5.9–6.5) \times 10^2$ K. Upon compression of the bubble to very small sizes (<1 μm), its potential energy turns into the kinetic energy of a high-speed (up to 10^3 m/s) jet directed toward the solid wall [46]. It is known that such jets can destroy the surface of quartz glass, forming microsized holes and other defects on the latter [47]. Acoustic measurements showed that the pulse pressure amplitude reaches 3×10^8 Pa at $\Phi = 40$ J/cm^2 and already 10^9 Pa at $\Phi = 100$ J/cm^2 (Fig. 6a).

The region with an elevated temperature (*1* in Fig. 7a), which simultaneously is a high-pressure

region, will mainly expand in the direction of free liquid (arrows *3* in Fig. 7a) due to the presence of a solid–liquid boundary, quite similar to the case when gas-vapor bubbles are generated by the hot end of the laser fiber [48]. The expansion rate of the heated area can be estimated by the measured pulse pressure amplitudes in accordance with the following expression [49]:

$$V = \sqrt{\frac{2}{3}\frac{\Delta p}{\rho^L}}, \quad (2)$$

where Δp is the pressure jump determined from the acoustic measurements. The Δp value is about 3×10^8 Pa for the laser energy density, $\Phi = 40$ J/cm^2 (Fig. 6a), and the expansion rate of Region 1 (Fig. 7a) should be about 450 m/s.

Let us note that the above-performed estimation of the temperature at the boundary between the sample surface and absorbing liquid was determined by Eq. (1) [7] without allowance for the absorption on the boundary itself [31], which is gradually increased under the multipulse laser etching mode due to the formation of an absorbing layer adsorbed on the surface and comprised of the photo- and thermal destruction products. The calculations showed that the surface absorption can be neglected at the laser energy densities, $\Phi < 50$ J/cm^2, upon using an aqueous dye solution.

LIBWE under the Mode of Volume and Surface Radiation Absorption

The role of surface absorption significantly increases in the LIBWE process with the addition of PEG in an aqueous dye solution. The experiments showed that the extensive laser-induced formation of carbon takes place in the course of laser etching under the condition when PEG is added in an aqueous dye solution, owing to the photo- and thermal destruction of dye and PEG. The formed carbon nano- and microparticles cover the surface of a produced crater (Fig. 3b) forming the area of near-surface laser radiation absorption (labeled as *2* in Fig. 7b). The Marangoni convection and the capture of nanoparticles from a volume of liquid by laser-induced bubbles promote the increased accumulation of the decomposition products at the area of laser exposure [50]. These bubbles (Fig. 3a) can be produced from the gases dissolved in water and also by the gaseous products (H_2, CO, CO_2, and CH_4) formed as a consequence of the oxidation and decomposition of dye and PEG. The absorption of part of laser radiation and the strong scattering in the surface layer (*2* in Fig. 7b) give rise to a decrease in the volume of strongly heated areas in the fluid (*1* in Fig. 7b) when compared to the case of pure dye (*1* in Fig. 7a). Therefore, the energy of the formed gas-vapor bubble is decreased. If it is considered that the addition of a surfactant (PEG) in an aqueous dye solution reduces the surface tension, then it becomes clear why the pulse pressure amplitudes in this case are substantially decreased (Fig. 6, Dye + PEG). As a result of these processes, the increased heating of the near-surface layer upon formation of structures on the surface of a transparent sample gives rise to an increase in the LIBWE rate, and a decrease in the cavitation leads to the formation of higher quality laser craters and tracks.

LIBWE under the Mode of Surface Radiation Absorption

The role of surface absorption in the LIBWE process becomes dominant when using an aqueous solution of $AgNO_3$ as a working fluid. Due to the photo- and thermal destruction of the precursor, the intensive laser-induced formation of metallic silver takes place in this case [51, 52]. The formed silver nano- and microparticles cover the surfaces of a sample (Fig. 5a) and of a formed crater (Fig. 5c), creating a region with a strong surface absorption of laser radiation.

In accordance with our assessment, the rate of formation of metallic silver on the sample surface at $\Phi =$ 26 J/cm^2 is about nm/s. According to calculations [53], 57% of the laser radiation is absorbed in a silver film with a thickness of 20 nm and 95% in a silver film with a thickness of 50 nm. The radiation absorption in a thin near-surface layer gives rise to its strong heating, which promotes the equivalently strong heating of the sample surface layer, which causes its rapid etching and destruction. During the laser pulse exposure, the fraction of the energy absorbed by a volume of liquid in this case is substantially lower than in the cases of using dye (LIBWE under the volume absorption mode) and dye with PEG (LIBWE under the volume and surface absorption mode). This leads to an even stronger suppression of the cavitation processes and pulse pressures accompanying them, as is proven by the results of the direct acoustic measurements (compare the pulse amplitudes in Figs. 6a and 6c).

It is important to note that the increased accumulation of laser-induced silver on the surface of a produced structure, as in the case of carbon formation, is promoted by the Marangoni convection and by the capture of nanoparticles from a volume of liquid by laser-induced bubbles [50].

In the case of LIBWE in a dye solution, the pulse pressure amplitude at $\Phi = 100$ J/cm^2 is about 10^9 Pa (Fig. 5a), which is at the level of the ultimate compressive strength of glass. However, the ultimate tensile strength of glass is much lower and approximately equals 3×10^7 to 10×10^7 Pa. Therefore, in order to surely be under the destruction threshold, it is neces-

sary to reduce the cavitation-induced pulse pressure 30 to 100 times. According to [32], the energy of acoustic pulses is proportional to Φ^2 in the region with $\Phi < 100$ J/cm^2. Since the acoustic energy is proportional to a square pressure, then the pulse pressure amplitude is proportional to Φ in the region with $\Phi <$ 100 J/cm^2. Hence, a specified decrease in the pulse pressure can be achieved by reducing the Φ value to $\Phi \sim 1$ J/cm^2, i.e., also by 30 to 100 times. However, this leads, in accordance with Eq. (1), to nearly the same strong decrease in the temperature of heating of the absorbing fluid and, as a result, also of the thin layer of glass (the thermal heating depth, d_T^G, for glass is about 80 nm), thereby substantially reducing the efficiency of etching.

Thus, to ensure the effective etching and avoidance of the cavitational destruction, it is sufficient to heat up only a thin near-surface liquid layer to the required temperature, T. The thickness of this layer is determined by the depth of thermal heating of a fluid during the pulse duration, which is estimated as $d_T^L \sim 50$ nm. As it was already noted, the thickness of a heated liquid layer in a dye solution is 10 μm. To reduce this layer to 50 nm, the absorption coefficient should be equal to $\alpha = 4 \times 10^5$ cm^{-1}. It is impossible to get such a value of the absorption coefficient using dye, since its limiting concentrations are used already in our case ($\alpha = 2 \times 10^3$ cm^{-1}). We propose an approach which consists of producing the absorbing sites (primarily, plasmonic nanoparticles) accumulated on the surface of glass and in the nearby volume of a fluid and which makes it possible to obtain higher values of the absorption coefficient and insignificant heating depths estimated at a level of 100 to 200 nm.

Consecutive increases in the rate and quality of etching upon the transition dye solution → dye + PEG solution → $AgNO_3$ solution observed in the experiment are connected with the following circumstances. Upon the transition dye solution → dye + PEG solution, the yield of carbon nano- and microparticles is increased by an order of magnitude. Owing to the Marangoni convection, they are adsorbed on the surface of a crater and, concentrating around it, form a layer of near-surface absorption and laser light scattering (*2* in Fig. 7b). As a result, the laser exposure gives rise to the pulsed heating of the area near the glass surface to temperatures larger than in the case of a solution without PEG. This increases the etching rate of the material of a transparent sample. The fluid volume amount heated up to high temperatures (*1* in Fig. 7b) is decreased due to the strong absorption and scattering in this near-surface layer too. The addition of PEG lowers the surface tension. In view of that, the energy of produced cavitation bubbles and the pulse pressure amplitudes are decreased (Fig. 6). In turn, this means that undesirable effects of the cavitational sample destruction are decreased and the etching quality is improved.

Upon the transition to a solution of $AgNO_3$, silver nano- and micro-particles are produced, the absorption cross section of which can exceed their geometric cross section by an order of magnitude due to plasmonic resonance. Owing to the Marangoni convection, silver nano- and microparticles form the laser radiation absorption layer (*2* in Fig. 7b) by adsorbing on the surface of a crater and by concentrating near it. Unlike the first two cases with dye, the volume heating of a fluid (*1* in Figs. 7a, 7b) can be neglected due to the weak laser radiation absorption in an aqueous solution of $AgNO_3$. Therefore, the volume of a fluid heated to high temperatures upon laser exposure is limited by the thickness of the near-surface absorption layer (according to our estimation, from 100 to 200 nm) and by the depth of its thermal heating (about 50 nm). The energy of produced cavitation bubbles and the pulse pressure amplitudes in this case are even smaller than in the case of using PEG (see Fig. 6). This allows one to achieve the good quality of etched craters and tracks (Fig. 4). In addition, a decrease in the pulse pressure upon the transition dye + PEG solution → $AgNO_3$ solution leads to the consequence that the destruction of the absorption layer itself under the influence of pulsed laser radiation is decreased. As a consequence of this and owing to the more efficient absorption of radiation, the pulsed heating of the near-surface layer and of the crater surface in the case of an $AgNO_3$ solution extends to significantly larger temperatures. This explains the observed increase in the etching rate of the material of a transparent sample.

Let us note that the adhesion of laser-induced absorbing sites on the surface of the formed crater (carbon or silver nano- and microparticles) may give rise to a decrease in the ultimate strength of a transparent sample due to the Rehbinder effect [54], which also increases the rate of the LIBWE process.

CONCLUSIONS

The processes of laser liquid etching and microstructuring of silicate glass by laser pulses with a wavelength of 527 nm and a duration of about 5 ns are studied experimentally with the use of different working fluids providing the following etching modes: volume (in a solution of dye), volume + surface (in a solution of dye and PEG), and surface (in an aqueous solution of $AgNO_3$).

The process of structure formation in a material during LIBWE processing is determined by the two different processes: chemical etching of the surface of the material by supercritical water (produced upon

rapid laser heating of a fluid) and shockwave (cavitational) destruction of the material. The LIBWE rate and the quality of the formed microstructures are determined by the dominant mechanism of LIBWE.

The cavitational destruction dominates upon using an aqueous dye solution for LIBWE, not allowing one to create well-reproducible craters and tracks. This is connected with the volume absorption in a fluid. The periodic heating of a sufficiently large (about 150 mm^3) volume of the fluid leads to the formation and cavitational collapse of high-energy bubbles, which are accompanied by large pulse-pressure amplitudes increasing the probability of the destruction of a crater or track.

It is possible to suppress the influence of cavitation by reducing the surface tension of a fluid and also by an increase in the absorption and scattering in the near-surface layer. This problem was successfully solved by the addition of PEG to dye, which leads to a decrease in the surface tension of a fluid and to an increase in the absorption of laser radiation by the near-surface layer due to the formation of carbon nano- and microparticles. An even more radical approach to the suppression of undesirable cavitation during LIBWE is based on using an aqueous solution of the silver precursor ($AgNO_3$) as an absorbing fluid. In this case, silver nanoparticles are gradually produced in the process of multipulse laser irradiation of a fluid volume due to the photo- and thermochemical decomposition of the precursor, causing the strong absorption on the surface of a generated structure. The cavitational destruction of a material is suppressed in this case, and the process of the chemical etching of glass surface by supercritical water becomes a dominant mechanism of LIBWE. Laser craters and tracks produced under this mode are characterized by high quality at a rather high etching rate (up to 10 nm/pulse).

Thus, the silver and carbon nanoparticles generated during the process of laser liquid etching and well absorbing the green laser light make it possible to implement a highly efficient and well-reproducible LIBWE technology for the fabrication of high-precision optical microstructures on the surface of advanced optical materials by using high-performance and reliable lasers with a wavelength of 527 nm.

ACKNOWLEDGMENTS

This work was supported by the Russian National Foundation (grant no. 14-13-01422) in the part of studies on mechanisms of the influence of lasers and supercritical fluids on optical materials and by the Government of the Russian Federation within the Program for State Support of Research Performed under the Supervision of Leading Scientists (grant no. 14.V25.31.0019) in the part of development of the technology for structuring of materials by the methods of laser nanoengineering.

REFERENCES

1. R. D. Schaeffer, *Fundamentals of Laser Micromachining* (CRC, Taylor Francis Group, Boca Raton, FL, 2012).
2. J. C. Ion, *Laser Processing of Engineering Materials: Principles, Procedure and Industrial Application* (Elsevier, Amsterdam, 2005).
3. Advances in *Laser Materials Processing: Technology, Research and Applications,* Ed. by J. Lawrence, J. Pou, D. K. Y. Low, and E. Toyserkani (CRC, Boca Raton, FL, 2010).
4. D. Bäuerle, *Laser Processing and Chemistry* (Springer, Berlin, Heidelberg, 2011).
5. V. P. Veiko, *Laser Microprocessing* (GU ITMO, St. Petersburg, 2005) [in Russian].
6. K. Zimmer, M. Ehrhardt, and R. Böhme, "Laser-induced backside wet etching: processes, results, and applications," in *Laser Ablation in Liquids: Principles and Applications in the Preparation of Nanomaterials,* Ed. by G. Yang (Pan Stanford, Singapore, 2012).
7. J. Wang, H. Niino, and A. Yabe, "One-step microfabrication of fused silica by laser ablation of an organic solution," Appl. Phys. A **68**, 111 (1999).
8. J. Wang, H. Niino, and A. Yabe, "Micromachining of quartz crystal with excimer lasers by laser-induced backside wet etching," Appl. Phys. A **69**, 271 (1999).
9. K. Zimmer and R. Böhme, "Precise etching of fused silica for refractive and diffractive micro-optical applications," Opt. Lasers Eng. **43**, 1349 (2005).
10. J.-Y. Cheng, M.-H. Yen, and T.-H. Young, "Crack-free micromachining on glass using an economic q-switched 532 nm laser," J. Micromech. Microeng. **16**, 2420 (2006).
11. J.-Y. Cheng, H.-Y. Chen, M. Z. Mousavi, and C. Y. Y. Chang, "Crack-free micromachining of glass ceramic using visible LIBWE," J. Laser Micro/Nanoeng. **8**, 253 (2013).
12. S. I. Dolgaev, A. A. Lyalin, A. V. Simakin, V. V. Voronov, and G. A. Shafeev, "Fast etching and metallization of via-holes in sapphire with the help of radiation by a copper vapor laser," Appl. Surf. Sci. **109–110**, 201 (1997).
13. S. I. Dolgaev, M. E. Karasev, L. A. Kulevskii, A. V. Simakin, and G. A. Shafeev, "Dissolution in a supercritical liquid as a mechanism of laser ablation of sapphire," Quantum Electron. **31**, 593 (2001).
14. B. N. Chichkov, C. Momma, S. Nolte, F. von Alvensleben, and A. Tunnermann, "Femtosecond, picosecond and nanosecond laser ablation of solids," Appl. Phys. A **63**, 109 (1996).
15. M. Ehrhardt, G. Raciukaitis, P. Gecys, and K. Zimmer, "Microstructuring of fused silica by laser-induced backside wet etching using picosecond laser pulses," Appl. Surf. Sci. **256**, 7222 (2010).

16. K. Zimmer and R. Böhme, "Laser-induced backside-Wet etching of transparent materials with organic and metallic absorbers," Laser Chem. **2008**, 170632 (2008). doi doi 10.1155/2008/170632

17. S. I. Dolgaev, A. A. Lyalin, A. V. Simakin, and G. A. Shafeev, "Etching of sapphire assisted by copper-vapour laser radiation," Quantum Electron. **26**, 65 (1996).

18. S. I. Dolgaev, A. A. Lyalin, A. V. Simakin, and G. A. Shafeev, "Fast etching of sapphire by a visible range quasi-Cw laser radiation," Appl. Surf. Sci. **96–98**, 491 (1996).

19. A. V. Simakin, E. N. Lubnin, and G. A. Shafeev, "Self-limiting of the thickness of diamond-like films deposited in the laser pyrolysis of liquid aromatic hydrocarbons," Quantum Electron. **30**, 263 (2000).

20. K. Zimmer, R. Bohme, D. Ruthe, and B. Raushenbach, "Backside laser etching of fused silica using liquid gallium," Appl. Phys. A **84**, 455 (2006).

21. B. Hopp, T. Smausz, T. Csizmadia, C. Vass, T. Csako, and G. Szabo, "Comparative study of different indirect laser-based methods developed for microprocessing of transparent materials," J. Laser Micro/Nanoeng. **5**, 80 (2010).

22. M.-H. Yen, C.-W. Huang, W.-C. Hsu, T.-H. Young, K. Zimmer, and J.-Y. Cheng, "Crack-free micromachining on glass substrates by visible LIBWE using liquid metallic absorbers," Appl. Surf. Sci. **257**, 87 (2010).

23. J. Zhang, K. Sugioka, and K. Midorikawa, "Laser-induced plasma-assisted ablation of fused quartz using the fourth harmonic of a Nd^+:YAG laser," Appl. Phys. A **67**, 545 (1998).

24. Y. Hanada, K. Sugioka, I. Miyamoto, and K. Midorikawa, "Double-pulse irradiation by laser-induced plasma-assisted ablation (LIPAA) and mechanisms study," Appl. Surf. Sci. **248**, 276 (2005).

25. B. Hopp, Cs. Vass, and T. Smausz, "Laser induced backside dry etching of transparent materials," Appl. Surf. Sci. **253**, 7922 (2007).

26. R. Böhme, K. Zimmer, and B. Rauschenbach, "Laser backside etching of fused silica due to carbon layer ablation," Appl. Phys. A **82**, 325 (2006).

27. R. Böhme and K. Zimmer, "Low roughness laser etching of fused silica using an adsorbed layer," Appl. Surf. Sci. **239**, 109 (2004).

28. A. M. Shakhov, A. A. Astaf'ev, N. N. Denisov, F. E. Gostev, I. V. Shelaev, A. N. Titov, and V. A. Nadtochenko, "Spherical gold nanoparticles and SiO_2/Au core/shell microparticles under intense femtosecond laser excitation: relaxation dynamics of gold nanoparticles and nanostructuring of borosilicate glass using SiO_2/Au microparticles," Quantum Electron. **44**, 852 (2014).

29. H. Niino, Y. Yasui, X. Ding, A. Narazaki, T. Sato, Y. Kawaguchi, and A. Yabe, "Surface micro-fabrication of silica glass by excimer laser irradiation of organic solvent," J. Photochem. Potobiol. A: Chem. **158**, 179 (2003).

30. C. Vass, J. Budai, Z. Schay, and B. Hopp, "Interpretation and modeling of laser-induced backside wet etching procedure," J. Laser Micro/Nanoeng. **5**, 43 (2010).

31. K. Zimmer, R. Bohme, M. Ehrhardt, and B. Rauschenbach, "Mechanism of backside etching of transparent materials with nanosecond UV-lasers," Appl. Phys. A **101**, 405 (2010).

32. M. Yu. Tsvetkov, V. I. Yusupov, N. V. Minaev, A. A. Akovantseva, P. S. Timashev, K. M. Golant, B. N. Chichkov, and V. N. Bagratashvili, "On the mechanisms of single-pulse laser-induced backside wet etching," Opt. Laser Technol. **88**, 17–23 (2017).

33. M. Yu. Tsvetkov, V. I. Yusupov, P. S. Timashev, K. M. Golant, N. V. Minaev, S. I. Tsypina, and V. N. Bagratashvili, "On the role of supercritical water in laser-induced backside glass wet etching," Sverkhkrit. Fluidy: Teor. Prakt. **11** (2), 14–27 (2016).

34. E. V. Smirnov, *Food Dyes, The Handbook* (Professiya, St. Petersburg, 2009) [in Russian].

35. M. Snehalatha, C. Ravikumar, N. Sekar, V. S. Jayakumar, and I. H. Joe, "FT-Raman, IR and UV-visible spectral investigations and ab initio computations of a nonlinear food dye amaranth," J. Raman Spectrosc. **39**, 928 (2008).

36. V. I. Yusupov, V. V. Bulanov, V. M. Chudnovskii, and V. N. Bagratashvili, "Laser-induced hydrodynamics in water-saturated tissue. 3. Optoacoustic effects," Laser Phys. **24**, 015601 (2014).

37. A. E. Siegman, *Lasers* (Univ. Science Books, Oxford, UK, 1986).

38. A. C. Ferrari and J. Robertson, "Resonant raman spectroscopy of disordered, amorphous, and diamondlike carbon," Phys. Rev. B **64**, 075414 (2001).

39. A. C. Ferrari and J. Robertson, "Raman spectroscopy of amorphous, nanostructured, diamond-like carbon, and nanodiamond," Phil. Trans. R. Soc. London A **362**, 2477 (2004).

40. According to [6] (K. Zimmer, M. Ehrhardt, and R. Böhme, "Laser-induced backside wet etching: processes, results, and applications," in *Laser Ablation in Liquids: Principles and Applications in the Preparation of Nanomaterials,* Ed. by G. Yang (Pan Stanford, Singapore, 2012)) we can observe structures with good surface quality during hydrocarbon etching...

41. M. Yu. Tsvetkov, V. N. Bagratashvili, V. Ya. Panchenko, A. O. Rybaltovskii, M. I. Samoilovich, and M. A. Timofeev, "Plasmon resonances of silver nanoparticles in silica based meso-structured films," Nanotechnol. Russ. **6**, 619 (2011).

42. A. O. Rybaltovskii, V. I. Gerasimova, N. V. Minaev, V. I. Sokolov, P. S. Timashev, E. A. Troitskaya, V. V. Firsov, V. I. Yusupov, and V. N. Bagratashvili, "Laser-induced formation of structures of silver nanoparticles in fluoracrylate films impregnated with AG(HFAC)COD molecules," Nanotechnol. Russ. **5**, 435 (2010).

43. A. O. Rybaltovskii, S. S. Ilyukhin, N. V. Minaev, P. S. Timashev, V. I. Yusupov, and V. N. Bagratashvili, "Dynamics of a photothermal self-assembly of plas-

mon structures in polymer films containing gold and silver precursors," Nanotechnol. Russ. **9**, 227 (2014).

44. U. Kreibig and M. Vollmer, *Optical Properties of Metal Clusters* (Springer, New York, 1995).

45. A. Yu. Olenin and G. V. Lisichkin, "Metal nanoparticles in condensed media: preparation and the bulk and surface structural dynamics," Russ. Chem. Rev. **80**, 605 (2011).

46. A. Vogel, W. Lauterborn, and R. Timm, "Optical and acoustic investigation of the dynamics of laser-produced cavitation bubbles near a solid boundary," J. Fluid Mech. **206**, 299 (1989).

47. V. I. Yusupov, V. M. Chudnovskii, and V. N. Bagratashvili, "Laser-induced hydrodynamics in water-saturated biotissues. 2. Effect on delivery fiber," Laser Phys. **21**, 1230 (2011).

48. V. I. Yusupov, V. M. Chudnovskii, and V. N. Bagratashvili, "Laser-induced hydrodynamics in water-saturated biotissues. 1. Generation of bubbles in liquid," Laser Phys. **20**, 1641 (2010).

49. A. Prosperetti and M. S. Plesset, "Vapour-bubble growth in a superheated liquid," J. Fluid Mech. **85**, 349 (1978).

50. V. I. Yusupov, S. I. Tsypina, and V. N. Bagratashvili, "Trapping of nanoparticles in a liquid by laser-induced microbubbles," Laser Phys. Lett. **11**, 116001 (2014).

51. U. Kreibig, M. Gartz, A. Hilger, H. Hovel, M. Quinten, and D. Wagner, "A short survey of optical properties of metal nanostructures," in *Functional Properties of Nanostructured Materials,* Ed. by R. Kassing (Springer, 2005).

52. A. Yu. Olenin, "Mechanisms of metal nanoparticle formation," Nanotechnol. Russ. **7**, 238 (2012).

53. V. S. Brunov, O. A. Podsvirov, A. I. Sidorov, and D. V. Churaev, "Formation of silver thin films and nanoparticles inside and on the surface of silver-containing glasses by electron irradiation," Tech. Phys. **59**, 1215 (2014).

54. A. I. Malkin, "Regularities and mechanisms of the Rehbinder's effect," Colloid J. **74**, 223 (2012).

Translated by O. Kadkin